Long-term light and period variations in the supersoft X-ray source V617 Sgr

Lei Zang[a,b,c], Ergang Zhao[a,b,c,d], Eduardo Fernández-Lajús[e,f], Ahmed Waqas Zubairi[a,b,c], Nopphadon Sarotsakulchai[g]

[a] *Yunnan Observatories, Chinese Academy of Sciences (CAS), P. O. Box 110, 650216 Kunming, P. R. China*
[b] *Key Laboratory of the Structure and Evolution of Celestial Objects, Chinese Academy of Sciences, P. O. Box 110, 650216 Kunming, P. R. China*
[c] *University of Chinese Academy of Sciences, No.1 Yanqihu East Rd, Huairou District, 101408, Beijing, P. R. China*
[d] *Center for Astronomical Mega-Science, Chinese Academy of Sciences, 20A Datun Road, Chaoyang District, Beijing, 100012, P. R. China*
[e] *Facultad de Ciencias Astronómicas y Geofísicas – Universidad Nacional de La Plata, Paseo del Bosque S/N – B1900FWA, La Plata, Argentina*
[f] *Instituto de Astrofísica de La Plata (CCT La Plata – CONICET/UNLP), B1900FWA, La Plata, Argentina*
[g] *National Astronomical Research Institute of Thailand, 260 Moo 4, T. Donkaew, A. Maerim, Chiangmai 50180, Thailand*

Abstract

V617 Sgr is one of the Galactic counterparts of supersoft X-ray sources as a member of the V Sagittae class, where a massive white dwarf is accreting material from its stellar companion and forming an accretion disk. Since 2014, we have monitored it for about nine years with the $2.15m$ telescope at CASLEO. It is found that the light curve shows obviously fluctuations and flickering, which imply the presence of actively hot spots on the accretion disk. Meanwhile, the flat-bottomed depressions can be explained by the presence of circumbinary material. By collecting all available eclipse times from the literature together with 149 newly determined times of light minimum, we constructed the O-C diagram and analyzed the variations in the orbital period of the eclipsing binary V617 Sgr. It is confirmed that the orbital period is increasing continuously with a rate of $\dot{P} = +1.68(3) \times 10^{-7} d \cdot yr^{-1} = +0.0145(3) s \cdot yr^{-1}$. A cyclic variation is detected to be superimposed on the period increase with an amplitude of $4.6min$ and a period of $26yr$. The continuous period increase is largely due to mass transfer from the donor secondary on its Kelvin–Helmholtz time-scale, while wind mass loss from the accretion disk surrounding the white dwarf may also contribute on the period change. In this case, the mass-transfer rate of V617 Sgr is estimated to be in the range of about 0.575×10^{-6} to $2.25 \times 10^{-6} M_{\odot} \cdot yr^{-1}$ and the mass-accretion rate is less than $1.59 \times 10^{-6} M_{\odot} \cdot yr^{-1}$. The cyclic change can be explained by the presence of a third body or magnetic activity cycles of the secondary.

Keywords: binaries: close – binaries: eclipsing – stars: evolution – stars: individual (V617 Sgr).

1. Introduction

V617 Sgr is an eclipsing supersoft X-ray source and has double eclipses with an orbital period of $0.207d$. The median values of magnitude and UBV colors are $V = 14.72mag$, $B - V = -0.05$ and $U - B = -0.79$ (Steiner et al. 1999). The U-B and B-V colors without any systematic variation suggest a very high temperature. Moreover, the optical high/low state has been observed and the primary eclipse becomes shallower at high state. An excursion of about 1.7mag has been observed by Steiner et al. (1999). It is seen that the depth of the primary eclipse is about 0.7mag at low state, while it is only 0.3mag at high state. In addition to the periodic modulation, there is also flickering in V617 Sgr. Steiner et al. (1999) has observed a power excess in the range of 17-27 minutes. Such a flickering and the optical high/low state have also been reported for V Sge (Herbig et al. 1965; Simon 1996; Robertson et al. 1997).

Strong emission lines of highly ionized species dominate the optical spectrum of V617 Sgr. Lines of *HeII* and the Balmer series can also be seen in emission, while *HeI* lines are weak or absent (Cieslinski et al. 1999). The lines in the optical spectrum of V617 Sgr and their relative intensities are remarkably similar to the V Sge stars. Deep absorption structures appear in the Balmer lines, which has also been observed in V Sge (Herbig et al. 1965; Cieslinski et al. 1999). The features, such as a strong $HeII\lambda$4686Å line ($HeII\lambda$4686Å/$H\beta$ flux ratio $\sim$ 2.9) together with other high excitation heavy element lines, are comparable with those presented by WX Cen, but not usually seen in cataclysmic

Email address: zanglei@ynao.ac.cn (Lei Zang)

variables (Cieslinski et al. 1999). The orbital line profile variations are similar to those seen in V Sge and WX Cen (Herbig et al. 1965; Williams et al. 1986; Diaz & Steiner 1995; Diaz 1999). Additionally, no sign of the donor secondary spectrum that could be used to constrain the secondary mass is also seen in V617 Sgr, as usual for the V Sge stars.

The spectrum of V617 Sgr also variances significantly between its optical high and low states. $H\alpha$ emission becomes stronger and broader at high state. This dramatic change in spectroscopic properties indicates a much stronger and faster wind at high state. The Doppler imaging and the orbital flux variation in $HeII$, as well as the self-absorption in $H\beta$, suggest the presence of the hot-spot and ionized gas flowing over the disk (Cieslinski et al. 1999; Steiner et al. 1999). This is consistent with the idea that a high and asymmetric rim exists associated with the accretion disk, similar to the proposed ones for the supersoft X-ray binary (Meyer-Hofmeister et al. 1997). In this case, the optically thick rim may be illuminated and ionized by the central source. Such a configuration is supported by the photometric and spectroscopic observations for V617 Sgr (Cieslinski et al. 1999; Steiner et al. 1999).

V617 Sgr was included in Wolf-Rayet (W-R) star catalogs under number 109 by van der Hucht et al. (1981), and then classified as a WN3 W-R star (van der Hucht et al. 1988; Conti & Vacca 1990). However, the classification of V617 Sgr as a W-R star was questioned (Lundstrom & Stenholm 1984, 1989), and its masses are far too low for a Population I W-R star (Cieslinski et al. 1999; Steiner et al. 1999). From the photometric point of view, the light curve of V617 Sgr is quite similar to those of V Sge, CAL 87 and QR And (Meyer-Hofmeister et al. 1997, 1998; Patterson et al. 1998). From the spectroscopic point of view, the highly ionized species emission lines in the compact binary supersoft X-ray sources and their intensities are basically same as those in V617 Sgr. Furthermore, the optical high/low state has also been reported for some supersoft X-ray sources. Therefore, due to these strong similarities, Steiner & Diaz (1998) proposed that V617 Sgr belongs to a small group denominated the V Sge stars, which are the X-ray quiet galactic counterpart of the supersoft X-ray sources seen in the Magellanic Clouds (Kahabka & van den Heuvel 1997).

The aim of this paper is to study the evolution of V617 Sgr via photometric observations. In Section 2, we describe observations and Section 3 is analysis of the observational results. Discussion and conclusions are given in Section 4.

2. Observations

The observations of V617 Sgr newly reported here were performed during 15 nights between 2014 March and 2022 August with the "Jorge Sahade" 2.15-m telescope using a Roper Scientific Versarray 2048B CCD camera. This telescope is located at the Complejo Astronómico El leoncito (CASLEO) observatory in San Juan, Argentina (henceforth, CASLEO-2.15). The broadband R and I filters of the Johnson-Cousins system was used. The observation for each night is shown in Figure 1. The detailed description of the adopted observational strategy and data reduction can be found in Agarwal et al. (2019).

In addition, the photometric observations used in this work were also collected by the American Association of Variable Star Observers (AAVSO[1]) database. Finally, 149 eclipse times were completed via fitting the CASLEO-2.15 and AAVSO light curves using the least-squares method in this study, which are tabulated in Table 1. The light curves observed on 2014 March 30, August 07 and 2017 June 26 with CASLEO-2.15 are hardly used to determine the eclipse times due to their incomplete coverage and peculiar shape. The data acquired on 2016 June 11 is a complete light curve covering an orbital period, so two eclipse times (i.e. primary and secondary eclipse) were extracted from it. Therefore, 13 times of minimum light were determined by fitting the CASLEO-2.15 light curves.

[1] https://www.aavso.org/databases

Table 1: 149 newly determined eclipse timings for V617 Sgr using CASLEO-2.15 and AAVSO data in this study. The eclipse timings with an asterisk are obtained from CASLEO-2.15 data.

Eclipse timings (HJD)	Errors (d)	E	O-C (d)	Eclipse timings (HJD)	Errors (d)	E	O-C (d)	Eclipse timings (HJD)	Errors (d)	E	O-C (d)
2456748.89045*	0.00016	47643.0	0.07536	2457905.32017	0.00098	53225.0	0.10056	2459074.49706	0.00102	58868.5	0.13219
2456817.67487	0.00039	47975.0	0.08044	2457906.15265	0.00036	53229.0	0.10438	2459074.59703	0.00049	58869.0	0.12857
2456817.88224	0.00105	47976.0	0.08065	2457906.25679	0.00077	53229.5	0.10494	2459075.63248	0.00028	58874.0	0.12819
2456818.61104	0.00034	47979.5	0.08436	2457907.18783	0.00018	53234.0	0.10373	2459076.66954	0.00054	58879.0	0.12941
2456818.71215	0.00074	47980.0	0.08189	2457908.22395	0.00040	53239.0	0.10401	2459078.64013	0.00086	58888.5	0.13192
2456818.81668	0.00187	47980.5	0.08284	2457992.54415*	0.00037	53646.0	0.10736	2459080.60473	0.00030	58898.0	0.12843
2456818.91943	0.00032	47981.0	0.08199	2457996.68635	0.00079	53666.0	0.10623	2459081.64034	0.00050	58903.0	0.12821
2456819.74652	0.00043	47985.0	0.08042	2458001.65485	0.00073	53690.0	0.10272	2459082.67791	0.00046	58908.0	0.12995
2456821.81689	0.00078	47995.0	0.07913	2458007.66899	0.00071	53719.0	0.10903	2459083.60943	0.00013	58912.5	0.12921
2456822.85575	0.00056	48000.0	0.08215	2458016.57767*	0.00024	53762.0	0.10954	2459084.64754	0.00102	58917.5	0.13150
2456823.68669	0.00054	48004.0	0.08442	2458289.83122*	0.00023	55081.0	0.11022	2459402.76155*	0.00036	60453.0	0.14103
2456823.78613	0.00126	48004.5	0.08028	2458704.58707	0.00029	57083.0	0.11834	2459414.57043	0.00104	60510.0	0.14141
2456824.62110	0.00073	48008.5	0.08658	2458709.55760	0.00095	57107.0	0.11686	2459414.77903	0.00148	60511.0	0.14285
2456825.75739	0.00065	48014.0	0.08346	2458712.56396	0.00076	57121.5	0.11930	2459425.75548	0.00130	60564.0	0.13946
2456826.58498	0.00031	48018.0	0.08238	2458717.53970	0.00084	57145.5	0.12305	2459435.70109	0.00055	60612.0	0.14107
2456826.79189	0.00042	48019.0	0.08213	2458718.56980	0.00013	57150.5	0.11731	2459440.67377	0.00136	60636.0	0.14175
2456827.62489	0.00111	48023.0	0.08646	2458736.49182	0.00046	57237.0	0.11942	2459441.71046	0.00030	60641.0	0.14261
2456827.72370	0.00066	48023.5	0.08168	2458736.59500	0.00132	57237.5	0.11901	2459442.74235	0.00052	60646.0	0.13866
2456829.80034	0.00034	48033.5	0.08666	2458737.52714	0.00054	57242.0	0.11890	2459446.68089	0.00072	60665.0	0.14104
2456830.73116	0.00037	48038.0	0.08522	2458738.56380	0.00064	57247.0	0.11972	2459453.72377	0.00054	60699.0	0.14025
2456832.79692	0.00052	48048.0	0.07932	2458739.49844	0.00125	57251.5	0.12212	2459463.67196	0.00047	60747.0	0.14444
2456859.72780*	0.00015	48178.0	0.07853	2458739.59799	0.00128	57252.0	0.11808	2459465.63891	0.00097	60756.5	0.14330
2456873.61287*	0.00028	48245.0	0.08343	2458741.56840	0.00094	57261.5	0.12041	2459790.16830	0.00026	62323.0	0.14605
2456884.59344*	0.00024	48298.0	0.08416	2458742.50036	0.00051	57266.0	0.12011	2459790.89485	0.00052	62326.5	0.14752
2457156.19682	0.00044	49609.0	0.09200	2458744.57195	0.00027	57276.0	0.12004	2459790.99520	0.00028	62327.0	0.14429
2457156.29609	0.00046	49609.5	0.08769	2458745.50395	0.00190	57280.5	0.11979	2459798.96812	0.00029	62365.5	0.14130
2457157.12210	0.00044	49613.5	0.08503	2458746.54251	0.00072	57285.5	0.12251	2459799.07411	0.00043	62366.0	0.14369
2457157.23159	0.00050	49614.0	0.09093	2458748.50700	0.00037	57295.0	0.11892	2459810.67608	0.00035	62422.0	0.14434
2457515.22111	0.00038	51342.0	0.09639	2458762.49560	0.00076	57362.5	0.12377	2459812.54328*	0.00027	62431.0	0.14703
2457530.75801	0.00031	51417.0	0.09580	2458763.53192	0.00062	57367.5	0.12425	2459812.64187	0.00031	62431.5	0.14204
2457531.79393	0.00071	51422.0	0.09589	2458766.53062	0.00042	57382.0	0.11904	2459812.74743	0.00058	62432.0	0.14402
2457532.83199	0.00102	51427.0	0.09811	2458767.56571	0.00026	57387.0	0.11829	2459812.95818	0.00024	62433.0	0.14760
2457533.86698	0.00050	51432.0	0.09727	2458768.50086	0.00079	57391.5	0.12120	2459813.05784	0.00035	62433.5	0.14368
2457534.79777	0.00068	51436.5	0.09581	2459061.54561	0.00050	58806.0	0.12865	2459814.61225	0.00017	62441.0	0.14433
2457534.90099	0.00042	51437.0	0.09544	2459061.64976	0.00135	58806.5	0.12921	2459814.71786	0.00079	62441.5	0.14636
2457535.73361	0.00042	51441.0	0.09940	2459063.51740	0.00077	58815.5	0.13235	2459816.68575	0.00025	62451.0	0.14616
2457539.87292	0.00036	51461.0	0.09537	2459063.61843	0.00104	58816.0	0.12980	2459817.71761	0.00083	62456.0	0.14219
2457540.91123	0.00060	51466.0	0.09785	2459064.65215	0.00063	58821.0	0.12769	2459819.58463	0.00023	62465.0	0.14471
2457542.77418	0.00064	51475.0	0.09630	2459065.48134	0.00045	58825.0	0.12821	2459819.68736	0.00075	62465.5	0.14386
2457542.87730	0.00171	51475.5	0.09584	2459065.68847	0.00058	58826.0	0.12818	2459825.59413	0.00034	62494.0	0.14638
2457543.70668	0.00080	51479.5	0.09655	2459066.51808	0.00053	58830.0	0.12912	2459825.69935	0.00134	62494.5	0.14802
2457543.81042	0.00067	51480.0	0.09671	2459066.72552	0.00040	58831.0	0.12939	2459832.63652	0.00059	62528.0	0.14510
2457543.91482	0.00034	51480.5	0.09752	2459067.65593	0.00120	58835.5	0.12755	2459836.57420	0.00069	62547.0	0.14661
2457550.64785*	0.00024	51513.0	0.09763	2459068.69526	0.00146	58840.5	0.13105	2459837.61042	0.00069	62552.0	0.14700
2457550.75572*	0.00027	51513.5	0.10192	2459069.52113	0.00152	58844.5	0.12826	2459841.54760	0.00028	62571.0	0.14801
2457551.99543	0.00120	51519.5	0.09863	2459069.62604	0.00055	58845.0	0.12957	2459841.64808	0.00109	62571.5	0.14491
2457552.09655	0.00016	51520.0	0.09616	2459070.66034	0.00070	58850.0	0.12804	2459843.61482	0.00053	62581.0	0.14357
2457577.78754*	0.00011	51644.0	0.09849	2459071.48810	0.00060	58854.0	0.12714	2459847.55239	0.00055	62600.0	0.14497
2457663.55380*	0.00036	52058.0	0.09773	2459071.69572	0.00066	58855.0	0.12760	2459853.56285	0.00046	62629.0	0.14759
2457905.21910	0.00031	53224.5	0.10307	2459072.63053	0.00052	58859.5	0.13015				

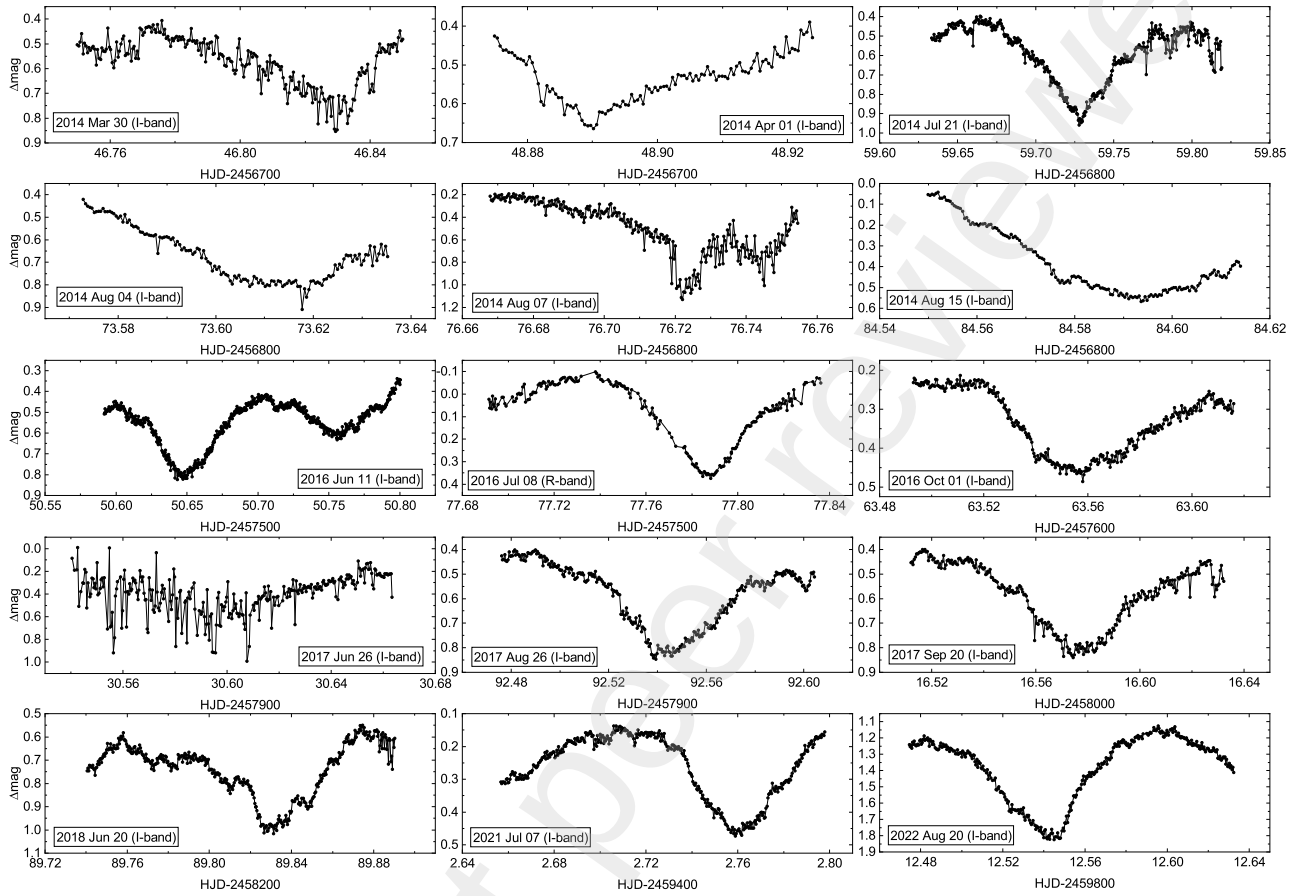

Figure 1: The differential light curves of distinct nights obtained with CASLEO-2.15 for V617 Sgr.

3. analysis and results

3.1. The light curve

Figure 1 shows the differential light curves of distinct nights for V617 Sgr. Long-term changes in brightness observed with CASLEO-2.15 using I filter are displayed in Figure 2, which include the data reported by Shi et al. (2014). Four important characteristics exhibited in the light curves are listed below. (1) In this study, the optical high/low state in V617 Sgr reported by Steiner et al. (1999) and Shi et al. (2014) was also found. As displayed in Figure 3, the brightness difference is up to 1.1*mag* in our observations. The primary eclipse becomes shallower at high state, the depth is only $\sim 0.3mag$, while that is $\sim 0.6mag$ at low state. (2) There are the flat-bottomed depressions during the primary eclipse. They are clearly seen in the light curves observed on 2014 April 01, August 07 and 2018 June 20. This may imply the presence of circumbinary material. (3) The light curves during the primary eclipse are asymmetric, that is, the times of ingress and egress to the eclipse are not equal. This provides a strong observational evidence for the existence of a high asymmetric rim over the disk (Steiner et al. 1999). (4) Obviously fluctuations and flickering also present, which may suggest the presence of active hot-spots on the accretion disk. A flickering with amplitude of 0.05*mag* and lasting for about 8*min* can be seen in the light curve obtained on 2018 June 20.

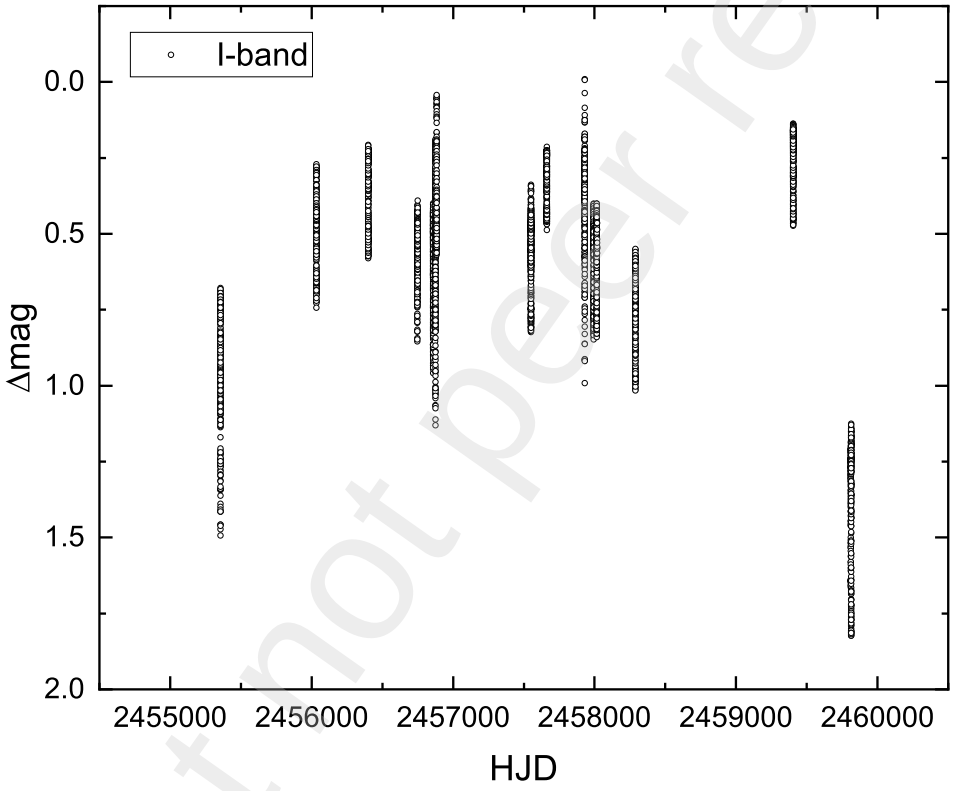

Figure 2: Long-term changes in brightness of V617 Sgr observed with CASLEO-2.15 including the data reported by Shi et al. (2014).

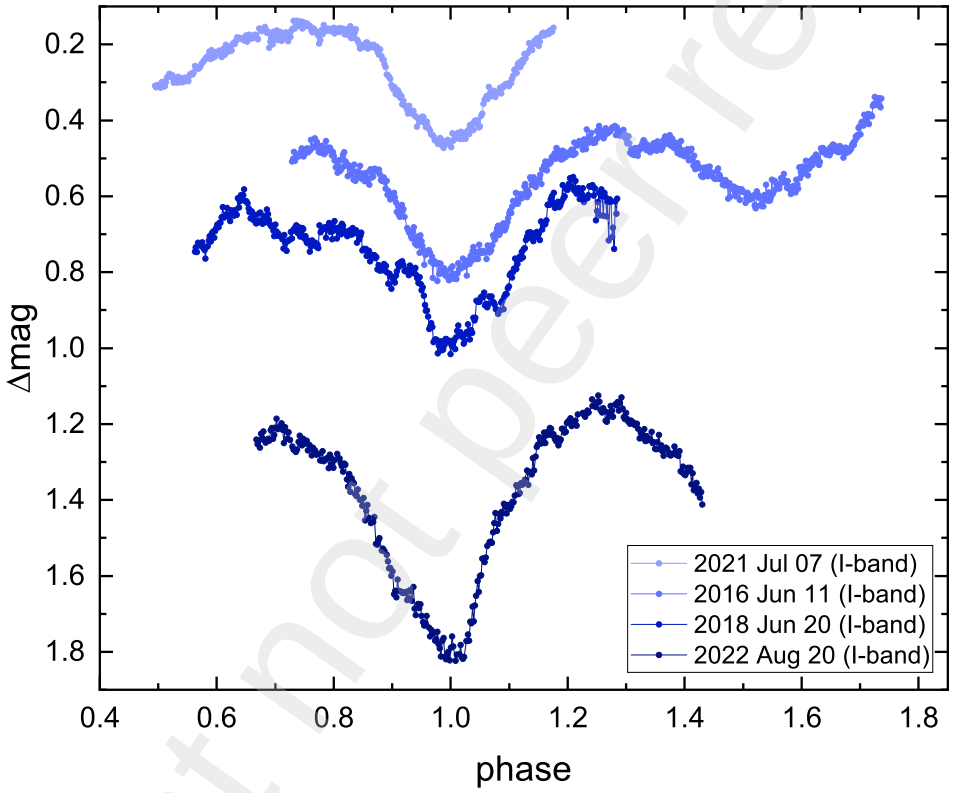

Figure 3: Light curves observed with the same filter showing the effects of different brightness states.

3.2. The orbital period change

The changes in orbital period of V617 Sgr was analyzed by using times of minimum light determined from the CASLEO-2.15 and AAVSO light curves and those published in Steiner et al. (1999), Steiner et al. (2006) and Shi et al. (2014). For V617 Sgr, epochs and O-C values were calculated for the available eclipse times according to the linear ephemeris from Steiner et al. (1999):

$$Min.I = HJD2446878.772 + 0.2071667E. \quad (1)$$

All O-C values can be fitted by a parabola model function (shown with the solid line in Figure 4) using the least-squares method, which represents the calculated quadratic ephemeris

$$Min.I = HJD2446878.770(1) + 0.20716613(6)E + 4.77(8) \times 10^{-11}E^2. \quad (2)$$

The dash line represents the quadratic ephemeris computed by Shi et al. (2014).

The ephemeris for the primary minimum of V617 Sgr has previously been given by Steiner et al. (1999), and then a long-term increase in the orbital period has been proposed by Steiner et al. (2006). However, Shi et al. (2014) reported that a cyclic component with a timescale of 4.5 yr may exist in the O-C diagram of V617 Sgr on the basis of increasing orbital periods.

In this work, the O-C diagram still shows a upward parabolic variation, which clearly illustrates that the orbital period is increasing. According to the quadratic term in Equation (2), the period is increasing at a rate of

$$\dot{P} = +4.60(8) \times 10^{-10} s \cdot s^{-1} = +1.68(3) \times 10^{-7} d \cdot yr^{-1}, \quad (3)$$

while the latest value is $+2.14 \times 10^{-7}\ d \cdot yr^{-1}$ determined by Shi et al. (2014) up to now. This discrepancy between previous values and our value is most likely caused by differences in the number of eclipse times and time spans.

In addition, the residuals related to the parabolic fit may present a cyclic oscillation. It can be described as:

$$Min.I = HJD2446878.7691(3) + 0.0032(3)\sin[0^\circ.0078(4)E + 66^\circ(23)]. \quad (4)$$

The corresponding amplitude of the cyclic variation is $A = 0.0032(3)d$ and the oscillating period is $P_3 = 26(1)yr$. Perhaps there is similar oscillation to that reported by Shi et al. (2014) in the residuals related to this cyclic oscillation. However, with the addition of the newly determined data in this study, that oscillation is inconspicuous and cannot be extracted. The confidence levels of fits mentioned above were estimated with analysis of variance (i.e. F-test), and the result implies that their significance levels are more than 99.99 per cent. The errors of fitted parameters are the unbiased standard errors covering the 68.27% confidence interval. And the error propagation formula was used to estimate the standard errors for the derived parameters.

4. Discussion and Conclusions

4.1. CAML by accretion disk wind in V617 Sgr

Steiner et al. (1999) proposed that the heavy element lines in the spectrum of V617 Sgr are more likely formed in a low density, extended envelope (probably a wind) surrounding the white dwarf. However, the envelope is probably formed from gas escaping from the system, which is suggested by the presence of the CNO emission lines. For the supersoft X-ray source with a higher mass-transfer rate ($\dot{M}_2 \gtrsim 10^{-8} M_\odot \cdot yr^{-1}$), a bright and optically thick hot-spot may be powered in the region of collision between the matter stream and the accretion disk, as presented in the photometric observations. The typical temperatures at the bright spot region may rise above 40000K. Yet such a hot region at a relatively low gravity location in the disk may lead to the radiative acceleration of a highly ionized wind (Cieslinski et al. 1999). Therefore, in this paper, the consequential angular momentum loss (CAML) mechanism driven by the accretion disk wind is considered for the evolution of V617 Sgr.

Steiner et al. (2006) derived a high mass for the white dwarf in V617 Sgr: $M_1 \geq 1.2M_\odot$ from the outburst (the optical high state) decline. Based on constraints on the component masses in V617 Sgr presented in Cieslinski et al. (1999), if the mass of the white dwarf is $M_1 \sim 1.2M_\odot$ and the orbital inclination is $i \sim 70^\circ$, then the donor secondary has a mass of $M_2 \sim 1.0M_\odot$. According to the Kepler's third law for a circular orbit, $M = \frac{0.0134d^3}{P^2}$, where $M = M_1 + M_2$

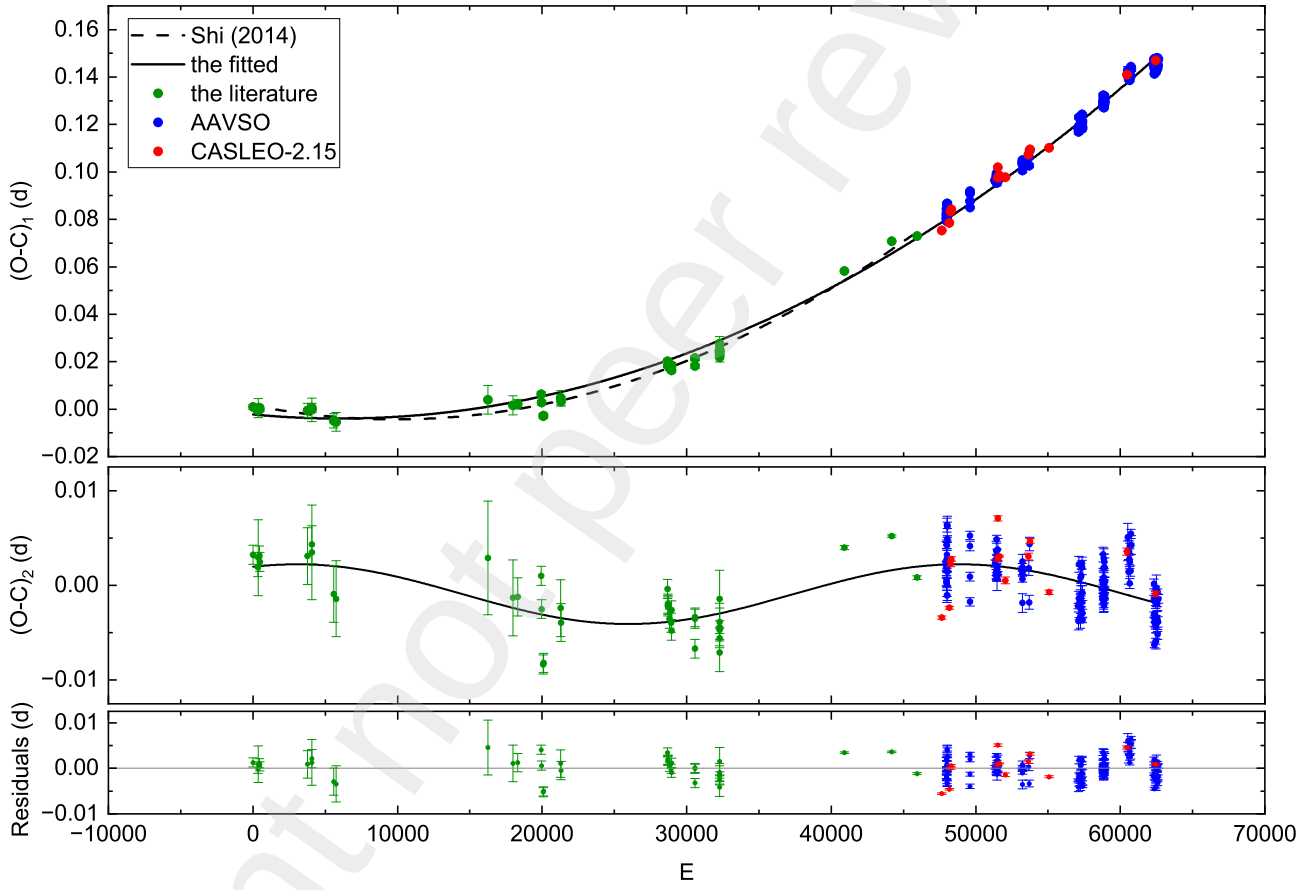

Figure 4: The O-C diagram for V617 Sgr (using an orbital period of 0.2071667*d* from the ephemeris of Steiner et al. (1999)).

is the total mass and $P = 0.20716613d$ is the orbital period, the binary separation $d = 1.92R_\odot$ is derived. Using the dependence of R_L/d on the mass ratio q ($q = \frac{M_2}{M_1}$),

$$\frac{R_L}{d} = \frac{0.49q^{\frac{2}{3}}}{0.6q^{\frac{2}{3}} + \ln(1 + q^{\frac{1}{3}})}, \tag{5}$$

found by Eggleton (1983), the Roche lobe radius of the donor secondary $R_L = 0.7R_\odot$ is calculated.

The mass-loss rate of the donor secondary is $\dot{M}_2 = \dot{M}_{2w} + \dot{M}_{2tr}$, where $\dot{M}_{2w}$ is the rate of the secondary's wind mass loss and $\dot{M}_{2tr}$ denotes the mass-transfer rate. For $\dot{M}_{2w}$, the model for enhanced stellar wind mass loss is proposed by Tout & Eggleton (1988),

$$\dot{M}_{2w} = -4 \times 10^{-13} \frac{R_2 L_2}{M_2} \{1 + 10^4 (\frac{R_2}{R_L})^6\} (M_\odot \cdot yr^{-1}), \tag{6}$$

with R_2, L_2 and M_2 in solar units. R_2 and L_2 is the radius and the luminosity of the donor secondary, respectively. Consequently, considering a Roche-filling star ($R_2 = R_L$), the rate of the stellar wind mass loss for the donor secondary is estimated as $\dot{M}_{2w} \simeq -8 \times 10^{-9} M_\odot \cdot yr^{-1}$. This is at least an order of magnitude smaller than the typical mass-transfer rate, thus it is negligible. Therefore, in this paper, we simply set $\dot{M}_2 \simeq \dot{M}_{2tr}$ and the total orbital angular momentum sink is approximately

$$\dot{J} \simeq \dot{J}_{CAML} = \dot{M}[j_d + j_1] \tag{7}$$

(King & Kolb 1995).

The specific orbital angular momentum of the white dwarf can be given by

$$j_1 = \frac{M_2^2}{M^2} d^2 \omega, \tag{8}$$

where ω is the orbital frequency ($\omega = 2\pi/P$). j_d is the average specific angular momentum of the mass-losing disk orbits relative to the white dwarf. It is assumed that $\dot{M} = \alpha \dot{M}_2$, which indicates that $\dot{M}_1 = (\alpha - 1)\dot{M}_2$, where $0 \leq \alpha \leq 1$ for V617 Sgr (King & Kolb 1995; Fang & Qian 2021). Here we do an approximation that $[j_d + j_1]$ satisfies the condition

$$j_1 \leq [j_d + j_1] \leq j(L_1). \tag{9}$$

$j(L_1) \simeq b^2\omega$ is the specific angular momentum at L_1 relative to the white dwarf, where b is the distance from L_1 to the white dwarf. Hence there is

$$|\dot{M}| j_1 \leq |\dot{J}_{CAML}| \leq |\dot{M}| j(L_1). \tag{10}$$

The total orbital angular momentum of the circular binary system is

$$J = \frac{M_1 M_2}{M} d^2 \omega, \tag{11}$$

so that

$$\alpha \frac{M_2 |\dot{M}_2|}{M_1 M} \leq \frac{|\dot{J}_{CAML}|}{J} \leq \alpha \frac{M}{M_1} \frac{b^2}{d^2} \frac{|\dot{M}_2|}{M_2}. \tag{12}$$

It can be written briefly as

$$\frac{\dot{J}_{CAML}}{J} = \nu \frac{\dot{M}_2}{M_2}, \tag{13}$$

where

$$\alpha \frac{M_2^2}{M_1 M} \leq \nu \leq \alpha \frac{M}{M_1} \frac{b^2}{d^2}. \tag{14}$$

Combined with the Kepler's third law for the circular orbit, the logarithmic differentiation of Equation (11) can be written as

$$\frac{\dot{J}}{J} = \frac{\dot{M}_1}{M_1} + \frac{\dot{M}_2}{M_2} - \frac{\dot{M}}{3M} + \frac{\dot{P}}{3P} = [(\alpha - 1)q + 1 - \frac{\alpha M_2}{3M}] \frac{\dot{M}_2}{M_2} + \frac{\dot{P}}{3P}, \tag{15}$$

so that

$$\nu\frac{\dot{M}_2}{M_2} \simeq [(\alpha-1)q+1-\frac{\alpha M_2}{3M}]\frac{\dot{M}_2}{M_2}+\frac{\dot{P}}{3P}. \tag{16}$$

The mass-transfer rate is estimated from Equation (16) as

$$|\dot{M}_2| \simeq 0.575-2.25\times10^{-6}M_\odot\cdot yr^{-1}. \tag{17}$$

If $\nu = 0$ (i.e. $\alpha = 0$), that is, the system will be in the simplest case of conservative mass transfer, then $\dot{M}_1 = -\dot{M}_2 = 1.59\times10^{-6}M_\odot\cdot yr^{-1}$ is an upper limit of the mass-accretion rate of the white dwarf.

Thus, the approximate timescale for the mass transfer from the secondary can be computed as $\tau_{M_2} = \frac{M_2}{|\dot{M}_2|} \simeq 6.3\times10^5 yrs$. Applying the formulas of the Kelvin-Helmholtz timescale

$$\tau_{KH} = 2\times10^7\frac{M_2^2}{R_2L_2} \tag{18}$$

and the nuclear timescale for stellar evolution

$$\tau_N = 10^{11}\frac{M_2}{L_2}, \tag{19}$$

$\tau_{KH} \simeq 1.2\times10^7 yrs$ and $\tau_N \simeq 4\times10^{10} yrs$ are estimated for the secondary. It is presented that the timescale of mass transfer is close to the Kelvin-Helmholtz timescale of the secondary. This reveals that the increasing orbital period may be caused by the mass transfer on the Kelvin-Helmholtz timescale of the secondary.

4.2. The explanations for the possible cyclic variation of orbital period

As discussed by Shi et al. (2014), the periodic component existing in O-C diagram of V617 Sgr may be caused by two mechanisms, that is the magnetic activity of the donor secondary (the Applegate's mechanism, Applegate 1992;190 Lanza & Rodonò 1999) or the light-travel-time effect due to the presence of a third component (Zhu et al. 2016; Liao191 & Sarotsakulchai 2019). According to the Applegate's mechanism, using the formula

$$\frac{\Delta P}{P} = \frac{4\pi A}{P_{mod}}, \tag{20}$$

where the semiamplitude and period of the sinusoidal fit to the observed O-C modulation is $A = 0.0032d$ and $P_{mod} = 26yr$ respectively, the fractional period change $\Delta P/P$ was computed to be 4.23×10^{-6}. Then using

$$\frac{\Delta P}{P} = -9\frac{\Delta Q}{M_2d^2}, \tag{21}$$

the variation of the quadrupole moment for the donor secondary was calculated to be $\Delta Q = 1.67\times10^{49} g\cdot cm^2$. This fits the typical ΔQ required to cause the magnetic activity for cataclysmic variables (Lanza & Rodonò 1999).

Considering the light-travel-time effect of a third body, the mass function for the third body in the hierarchical trisomy system is

$$f(M) = \frac{4\pi^2}{GP_3^2}(a_{12}\sin i_3)^3 = \frac{(M_3\sin i_3)^3}{(M_1+M_2+M_3)^2}, \tag{22}$$

where G is the gravitational constant, M_3 is the mass of the third body, and i_3 is the included angle between the outer orbital plane and the normal of the inner orbital plane. a_{12} is the orbital semi-major axis of the eclipsing binary relative to the barycenter of the triple system, which was calculated to be $a_{12}\sin i_3 = 0.55au$ with the projected formula $a_{12}\sin i_3 = cA$. When the included angle is $i_3 = 90°$, the minimum mass of the third body is estimated to be $M_{3,min} = 0.11M_\odot$ from Equation (22) and the orbital semi-major axis is $a_3 = 11au$. This implies that the third body may be an extremely low-mass star.

5. Acknowledgments

This work is supported by the National Key R&D Program of China (Grant No: 2022YFE0116800) and the National Natural Science Foundation of China (No. 11933008) and the basic research project of Yunnan Province (Grant No. 202201AT070092). We acknowledge with sincerest thanks the CASLEO telescope allocation committee and staff members and night assistants of CASLEO for their first class support. We thank the variable star observations from the AAVSO International Database contributed by observers worldwide and used in this research.

References

[1] Agarwal, A., Cellone, S. A., Andruchow, I., et al., 2019, MNRAS, 488, 4093
[2] Applegate, J. H., 1992, ApJ, 385, 621
[3] Cieslinski, D., Diaz, M. P., & Steiner, J. E., 1999, AJ, 117, 534
[4] Conti, P. S., & Vacca, W. D., 1990, AJ, 100, 431
[5] Diaz, M. P., 1999, PASP, 111, 76
[6] Diaz, M. P., & Steiner, J. E., 1995, AJ, 110, 1816
[7] Eggleton, P. P., 1983, ApJ, 268, 368
[8] Fang, X., & Qian, S., 2021, MNRAS, 501, 3046
[9] Herbig, G. H., Preston, G. W., Smak, J., & Paczynski, B., 1965, ApJ, 141, 617
[10] Kahabka, P., & van den Heuvel, E. P. J., 1997, ARA&A, 35, 69
[11] King, A. R., & Kolb, U., 1995, ApJ, 439, 330
[12] Lanza, A. F., & Rodonò, M., 1999, A&A, 349, 887
[13] Liao, W. P., & Sarotsakulchai, T., 2019, PASP, 131, 014202
[14] Lundstrom, I., & Stenholm, B., 1984, A&A, 138, 311
[15] Lundstrom, I., & Stenholm, B., 1989, A&A, 218, 199
[16] Meyer-Hofmeister, E., Schandl, S., Deufel, B., Barwig, H., & Meyer, F., 1998, A&A, 331, 612
[17] Meyer-Hofmeister, E., Schandl, S., & Meyer, F., 1997, A&A, 321, 245
[18] Patterson, J., Kemp, J., Shambrook, A., et al., 1998, PASP, 110, 380,
[19] Robertson, J. W., Honeycutt, R. K., & Pier, J. R., 1997, AJ, 113, 787
[20] Shi, G., Qian, S.-B., & Fernández Lajús, E., 2014, PASJ, 66, 8
[21] Simon, V., 1996, A&AS, 118, 421
[22] Steiner, J. E., Cieslinski, D., Jablonski, F. J., & Williams, R. E., 1999, A&A, 351, 1021
[23] Steiner, J. E., & Diaz, M. P., 1998, PASP, 110, 276
[24] Steiner, J. E., Oliveira, A. S., Cieslinski, D., & Ricci, T. V., 2006, A&A, 447, L1
[25] Tout, C. A., & Eggleton, P. P., 1988, MNRAS, 231, 823
[26] van der Hucht, K. A., Conti, P. S., Lundstrom, I., & Stenholm, B., 1981, SSRv, 28, 227
[27] van der Hucht, K. A., Hidayat, B., Admiranto, A. G., Supelli, K. R., & Doom, C., 1988, A&A, 199, 217
[28] Williams, G. A., King, A. R., Uomoto, A. K., & Hiltner, W. A., 1986, MNRAS, 219, 809
[29] Zhu, L. Y., Zhou, X., Hu, J. Y., et al., 2016, AJ, 151, 107